Published in final edited form as:
*J Microsc*. 2014 February ; 253(2): 83–92. doi:10.1111/jmi.12099.

# COMPACT NON-CONTACT TOTAL EMISSION DETECTION FOR *IN-VIVO* MULTI-PHOTON EXCITATION MICROSCOPY

**Christian A. Combs**[#1,#], **Aleksandr Smirnov**[#2], **Brian Glancy**[3], **Nader S. Karamzadeh**[4], **Amir H. Gandjbakhche**[4], **Glen Redford**[5], **Karl Kilborn**[5], **Jay R. Knutson**[2], and **Robert S. Balaban**[3]

[1] NHLBI Light Microscopy Facility, National Institutes of Health, Bethesda, Maryland 20892-1061

[2]NHLBI Laboratory of Molecular Biophysics, National Institutes of Health, Bethesda, Maryland 20892-1061

[3]NHLBI Laboratory of Cardiac Energetics, National Institutes of Health, Bethesda, Maryland 20892-1061

[4]NICHD Section on Biomedical Stochastic Physics, National Institutes of Health, Bethesda, Maryland 20892-1061

[5]Intelligent Imaging Innovations, Inc., Denver, CO 80216

[#] These authors contributed equally to this work.

## Summary

We describe a compact, non-contact design for a Total Emission Detection (c-TED) system for intra-vital multi-photon imaging. To conform to a standard upright two-photon microscope design, this system uses a parabolic mirror surrounding a standard microscope objective in concert with an optical path that does not interfere with normal microscope operation. The non-contact design of this device allows for maximal light collection without disrupting the physiology of the specimen being examined. Tests were conducted on exposed tissues in live animals to examine the emission collection enhancement of the c-TED device compared to heavily optimized objective-based emission collection. The best light collection enhancement was seen from murine fat (5×-2× gains as a function of depth), while murine skeletal muscle and rat kidney showed gains of over two and just under two-fold near the surface, respectively. Gains decreased with imaging depth (particularly in the kidney). Zebrafish imaging on a reflective substrate showed close to a two-fold gain throughout the entire volume of an intact embryo (approximately 150 μm deep). Direct measurement of bleaching rates confirmed that the lower laser powers (enabled by greater light collection efficiency) yielded reduced photobleaching *in vivo*. The potential benefits of increased light collection in terms of speed of imaging and reduced photo-damage, as well as the applicability of this device to other multi-photon imaging methods is discussed.

### Keywords

Two-photon microscopy; imaging; light collection

[#]Send correspondence to: Christian A. Combs, 9000 Rockville Pike, 10/6N-309, Bethesda, MD 20892-1061, Phone: (301) 496-3236, Fax: (301) 480-1477, combsc@nih.gov.

## Introduction

Multi-photon excitation microscopy (MPEM) (Denk *et al.*, 1990) is a powerful tool for studying biological processes *in vivo*. This type of imaging yields sub-cellular resolution and a means to interrogate cellular processes in a relatively non-invasive manner. Like most forms of high-resolution imaging, signal-to-noise ratio (SNR) is always a factor. This is particularly true for *in vivo* imaging, where the chromophores tend to be more limiting due to either expression or access issues, image averaging is limited by motion (Bakalar *et al.*, 2012, Schroeder *et al.*, 2010) and excitation power must be minimized to reduce photo-damage to the living tissue. These requirements place a premium on capturing all of the available emission light possible - to optimize SNR at a given excitation power level *in vivo*. A key feature of MPEM, whether it is used in fluorescence, multiple harmonic or even CARS imaging, is that the origin of the emitted signal is the diffraction-limited excitation spot. This means that all of the photons that exit the specimen are relevant, without a need for eliminating “out-of-focus” photons for slice selection required in techniques such as confocal microscopy. This is particularly helpful with increasing imaging depth, as scattered light becomes more prevalent (Centonze & White, 1998). Current commercial MPEM do not fully take advantage of this opportunity, since they only capture emitted light entering back through the same objective used for excitation and, in some cases, through a trans-condenser. Home-built systems have enabled collecting light missed by the objective through the use of parabolic mirror systems (Combs *et al.*, 2011, Combs *et al.*, 2007), fiber light guides (Engelbrecht *et al.*, 2009, McMullen *et al.*, 2011), hybrid objectives (Vucinic *et al.*, 2006), and trans-detection systems (Crosignani *et al.*, 2011, Engelbrecht et al., 2009, Crosignani *et al.*, 2012) but these devices have been generally limited by either their complexity or by limited access to the sample or by the low numerical aperture (N.A.) of wide-area objectives used. Among these designs, only the non-contact TED approach simultaneously allows for efficient light collection while minimizing the potential for altering the physiology of the sample and still permitting the use of commercial medium-N.A. objectives (0.75 to 1.0) (Combs et al., 2011). Although this design was shown to effectively capture approximately twice as much light as collected through the objective, the prototype relied upon an external optical subsystem that shunted excitation light to an objective mounted above the specimen on a separate stage beside an inverted microscope through a telescopic arm containing a complex mirror/relay lens system. In that design, a parabolic mirror surrounded the objective and sample under observation collected and directed emitted light to a bulky PMT mounted above the telescope arm. This system was relatively hard to mechanically stabilize and use, it required an external stage for z-translation and it did not take advantage of standard microscope features. In addition, the optical relay of the periscope increased light losses and group velocity dispersion. Further, the additional elements increased the chance for introduction of optical aberrations within the excitation pupil.

Here we test a design modification where the TED parabola surrounds the objective on a conventional upright two-photon microscope (Figure 1). This design retains the normal excitation path. Emission light collected by the parabola is now folded through a compact *conic telescope*, then combined with the emission from the objective, to reflect off an

oversized dichroic mirror and then be focused on a wide-area photomultiplier tube (PMT) within the microscope turret. While the ‘collapsed’ aperture used still exceeds that of the objective, considerable miniaturization was achieved, and the design path to an all-objective device (via, eg., future customized objective bodies) is made apparent.

One goal of this design was to add minimal complexity to a standard, live-animal imaging MPEM. We measure the detected emission gain on several tissues in live mice and upon a live intact zebrafish embryo placed on a protected silver mirror surface. The gain as a function of depth in these tissues and the practical benefit of collecting more emission light to reduce photo-bleaching is shown. Future directions for this device are discussed.

## Methods

### Compact TED Construction

The compact epiTED (c-TED) device (Figure 1) is built as a nose-piece for the 3i VIVO 2-Photon™ laser scanning microscope system (Intelligent Imaging Innovations, Inc., Denver, CO), which utilizes a Zeiss Axio Examiner Z1 upright microscope stand, beam expansion and attenuation/blanking optics, scan head, XY automated sample positioning stage, and SlideBook™ 5.0 acquisition software . A Chameleon Ultra II™ laser (Coherent Inc., Santa Clara, CA) is the source of near-IR femtosecond pulses at 80 MHz repetition rate.

The epiTED concept prototyped and tested in our earlier work (Combs et al., 2011) was substantially redesigned and optically folded for an upright microscope stand capable of moving the whole assembly in the vertical dimension, as opposed to the prior need to Z-scan the actual object. This refinement is essential for live-animal imaging.

This compact version of epiTED includes a custom nose-piece assembly for mounting the objective (Zeiss W Plan-Apochromat 20× / 1.0 N.A. water-immersion, infinity-corrected) that also holds the oversized IR-pass dichroic mirror, light gathering assembly, emission filters, protective shutter and a wide-area PMT (model H2431/R2083; Hamamatsu Photonics K.K., Japan) . This constitutes a wide aperture non-descanned detection pathway, gleaning some of the advantages described by Zinter and Levene (2001). The PMT was biased typically between -1 and -2 kV using a stabilized high-voltage power supply (PS350/5000V-25W from Stanford Research Systems, Inc., Sunnyvale, CA). Analog PMT output was conditioned with Hamamatsu inverting pre-amplifier unit model C7319 set for gain of 10^6 V/A, high-frequency bandwidth and connected directly to an available 14-bit A/D input of the VIVO™ 2-Photon™ imaging system.

The light gathering assembly consists of a custom electro-formed parabola mirror, coated inside with $SiO_2$ protected aluminum and mounted on an aluminum cylinder, polished on the inside. Parabolic shape (focal length) was chosen to collect the maximum amount of light emanating from the sample and not captured by microscope objective lens; the parabola apex was cut 1 mm below its focal point to help collect any photons that might escape slightly downward (e.g., from a convex-shaped sample). Fine threading is machined into the cylinder that holds the parabola so that the parabola can be raised for sample positioning and then lowered for focusing. For optimum performance, the parabola focal

point should approximately coincide with the bottom of the objective focus and thus its threaded mount allowed for manual adjustment (Figure 1, bottom-right).

All parts internal to the assembly were mirror-polished. Light gathered by the parabola (and objective collimated emission) was directed up to the main dichroic inside the nosepiece and reflected toward the PMT (Figure 1, upper-right). The conical telescope elements (Figure 1, bottom-left) were additionally silver-coated and buffed to a mirror finish (service of Metro Plating & Polishing, Inc., Kensington, MD).

Custom-sized high performance optics (the main rectangular 45° dichroic (p/n FF670-SDi01-34.8×46, Semrock Inc., Rochester, NY) and ∅2.5” near-IR-blocking emission filters were used). Notably, the dichroic was mounted on a slider so that it can be removed from the path, enabling wide-field fluorescence or transmitted illumination sample observation (Figure 1, middle-left).

A hollow reflective cone made of protected aluminum tape (not shown in Figure 1) was inserted between PMT shutter and the last optical element to channel any remaining scattered fluorescence towards the detector.

An important element in this system was that the front face of the objective, outside the *active* front lens element surface, was covered by an aluminum tape collar specifically angled to redirect upward scattered light toward the parabolic reflector (see yellow light rays in Figure 1, bottom-left). A significant amount of “minimally” scattered light emanates from the tissue to arrive just outside of the front lens active circumference.

A mirror-polished aluminum cylinder (not shown in Figure 1) was slipped over the objective body to minimize any light loss due to absorbance or scatter on its sides.

A piece of black heavy-duty cardboard (a mask) cut to block only light from the parabola was inserted in control experiments via a slot in the nosepiece, just above the objective back aperture. This was only used to determine the sole contribution of objective-collected light versus the parabola (for purposes of the gain calculation) and would not be used in normal operation.

## In Vivo Animal Imaging

**Image Acquisition—**All images were collected using the Slidebook 5.0 software (Intelligent Imaging Innovations, Inc., Denver, CO) and processed offline for background correction, registration and thresholding (see *Image Processing*). Typically two sets of data were collected, with laser on and off. In all cases gain was calculated from the integrated signal from each imaging plane for the imaging system as a whole (parabola and objective) and with objective alone (parabola emission collection blocked) data sets. It is important that such gain evaluation areas do not include dark regions, as they contain only noise and hence will yield no gain. In most cases laser dwell times were set to 2 μs/pixel and average of 5 samples per pixel but at times bidirectional scanning with 1.2 μs/pixel and 2 samples/pixel was necessary to reduce motion artifacts. Sample exposure to laser was minimized by means

of electro-optical beam blanking and kept to a level at which no visible photodamage to tissue occurred throughout the course of the whole experiment.

**Zebrafish Embryos—**Heterozygous *Tg(7×TCF-Xla.Siam:GFP)ia4* embryos (Morro et al. 2012) were generated by natural spawning and maintained at 28°C in standard embryo media (60 mg RedSea Coral Pro Salt per liter dd$H_2O$, Drs Foster and Smith Pet Supplies). Embryos at 28 hours post fertilization were anesthetized in Tricaine (Sigma, E10521) at a final concentration of 600 μM. For imaging, anesthetized embryos were held in 0.75% low-gelling temperature agarose (Cambrex, 50080), covered in embryo media and placed directly on reflective surface of a 25 mm protected silver mirror (PF10-03-P01, Thorlabs, Newton, NJ). Zebrafish images were acquired using 900 nm excitation light. All other imaging parameters were as outlined above.

**Mouse Skeletal Muscle and Fat—**C57BL/6 mice were prepared for imaging as described previously (Bakalar *et al*., 2012). Briefly, mice were anaesthetized and ventilated on a temperature-controlled surgical bed while the skin and fascia above the Tibialis anterior muscle were carefully removed. The mouse was then placed on the microscope stage with the leg coupled to the objective by an optical gel (Rothstein *et al.*, 2005). For fat imaging the point of focus was moved near or above the knee. For gain or bleaching studies, 50 μl of 4.2 mM di-8-[butyl] amino-napthylethylene-pyridinium-propyl-sulfonate (ANEPPS, Molecular Probes) or 100 μM tetramethylrhodamine, methyl ester perchlorate (TMRM, Molecular Probes), respectively, was injected into the jugular vein. Images were acquired using 800nm excitation light and a ∅2.0” 546 nm longpass interference emission filter. To assess signal gain, muscles were imaged with identical laser power settings and collected light intensity was quantified. For bleaching experiments, laser power settings were adjusted to achieve equal initial emission intensities and signal decay was followed.

**Rat Kidney—**Male Sprague-Dawley rats (5 months old, Harlan) were prepared for *in vivo* kidney imaging as described previously (Combs et al., 2011). Briefly, rats were anaesthetized and placed on a heated bed while the kidney was exteriorized and placed in a cup-like device for stability. ANEPPS (200 μl of 4.2 mM stock) was injected into the heparinized jugular vein to visualize the vasculature. The rat was transferred to the microscope stage where the kidney was coupled to the objective by an optical gel (as above).

## Image Processing

All image analysis was performed by custom written software in the IDL programming language (Exelis Visual Information Solutions, Boulder, Co). Gain is defined as the ratio of the light collected by the whole compact TED system (parabola + objective) to the light collected by the objective alone. In the cases where objective collected light was measured, a cardboard mask was inserted in the turret of the microscope that completely blocked emission light collected by the parabola mirror from reaching the PMT. Thresholding of images for intensity quantification was performed as previously described (Combs et al. 2011). Image registration for all experiments was conducted by 2D or 3D correlation analysis to align datasets before quantification and comparison of image stacks taken with

and without the parabola. In all cases, the region of interest measured avoided edges where the image was shifted as a result of re-alignment. Decay constants for quantification of bleaching level were fitted assuming a mono-exponential and a constant offset. Maximum projection images and movie files were generated using both Imaris (Bitplane Scientific Software, Zurich, Switzerland) and Metamorph (Molecular Devices, Sunnyvale, CA) software packages.

## Results

In general, the added signal from c-TED preserved image quality while it enhanced signal to noise in all preparations studied. We examined a wide variety of preparations to characterize the utility of the approach but also to explore its limitations with regard to geometry and tissue types (highly absorbent, scattering etc.). The last series of experiments was to demonstrate the efficacy of c-TED in reducing excitation power while maintaining signal to noise of labile *in vivo* samples.

The maximum intensity projections and single slice images shown in figures 2A,B and 4A,B, and C for fat, blood vessels skeletal muscle, zebrafish embryo and kidney demonstrate that the c-TED design shown in Figure 1 is capable of producing high quality images relative to a standard commercial two-photon microscope, *in vivo*. Figures 2 through 5 also show that the c-TED device is capable of collecting much more light than the objective alone, improving the signal-to-noise ratio. The amount of gain (defined as total light/objective alone ratio) in collection efficiency varies as a function of tissue type, depth and geometry of the sample. The highest gains observed were in the mixed tissue type seen in figures 2A and 2B near the knee of the mouse. The raw data from 2A can be seen in the form of histograms in figures 3A and 3B. In those images, gains were observed as high as ~ five-fold at the surface, decreasing to just greater than two-fold at a depth of 100 μm (Figure 3C). The five-fold gain we observed in the mixed tissue (dominated by fat which is highly scattering and weakly absorbing) image shown in figure 2 was the largest observed in any of the tissues we imaged. Other mixed tissue images we took in a similar environment (but with subtly different geometry) showed less gain (N=3, mean=3.6, max=5, min=2.8 for gain in the 3D volumes measured).

Figure 4 shows comparisons in other mammalian tissue types and in a zebrafish embryo. For all of these samples, maximal gains were around two-fold or higher. In skeletal muscle, gains varied as a function of depth from a value of approximately 2.5 fold to around two-fold at 300 μm depth (Figure 5a). In zebrafish embryos the gains were found to be slightly less than two-fold throughout the embryo volume (Figure 5a). In kidney, a much more light absorbing tissue, gains were found to vary strongly with depth from a value of two-fold to a 1.4 fold at a depth of 200 μm (Figure 5a and 5b). Figure 6 demonstrates that the bleaching rate in time course imaging can be reduced using c-TED while preserving the same detected SNR. In this case, the laser power was adjusted to give the same initial image intensity for c-TED and the objective alone in a TMRM study of mouse skeletal muscle, *in vivo*. To match the signal level first obtained with ~59% of available laser power (collected with the objective alone) it only required ~40% laser power using c-TED, consistent with the approximate two-fold increase in signal at constant power observed above (i.e. two fold

efficiency allows 41% ($\sqrt{2}=1.41$ vs. 1.0) power reduction). Efficient use of laser power by c-TED permitted us to demonstrate a significant decrease in TMRM bleaching rate with c-TED (when compared to the objective alone) -- at the same detected signal intensity (Figure 6B).

## Discussion

Herein a strategy is demonstrated for implementing a compact epiTED (c-TED) capability in a standard commercially available MPEM microscope while retaining near optimal light collection capabilities. Improved light collection increases the temporal efficiency of image collection. This is particularly important ***in vivo,*** where motion makes image averaging difficult and limitations in chromophore concentration and/or extinction are common. Another advantage of c-TED is to maintain the SNR yet decrease the laser power required, minimizing photo-damage and bleaching effects (Figure 6).

All experiments conducted here were done in living anesthetized animals with demonstrated blood flow within the field of view. As we have seen in previous studies, in most cases sample drift was detected and correlation analysis was needed to re-register images for comparisons (Bakalar et al., 2012, Schroeder et al., 2010). No dynamic motion tracking was used for these studies. The successful use of c-TED on a variety of preparations demonstrates the utility of this approach for *in vivo* imaging (in contrast with several other methods mentioned in the Introduction), since it did not need to contact the sample to achieve gains in light collection. It has been our experience that physical contact of devices to restrict motion (see (Bakalar et al., 2012, Schroeder et al., 2010)) or to collect light impede tissue blood flow and physiological function; thus, we put a high priority on designs for *in vivo* imaging that minimize tissue contact.

Other designs for increasing light collection have proven effective, with and without tissue contact. Engelbrecht et al. 2009 have shown that supplementary fiber optic light collection is effective at capturing more light. In theory, due to the low N.A. of optical fibers, it cannot achieve the gain of a parabolic mirror design (Combs et al., 2011, Combs et al., 2007); further, fiber contact with the tissue is required in current designs. McMullen et al. (2010) showed an effective design with a ring of fiber optics apertures that could increase the efficiency of a low N.A. (0.4) objective by 20 fold over a large field of view. However, with typical MPEM objectives having N.A. ≈ 1.0 the gain with this system dropped to only 10 to 20% (McMullen & Zipfel, 2010). For supplementing efficient MPEM objectives with high N.A., c-TED performed much better with a simpler optical arrangement. Crosignani et al. 2011 and 2012 presented a novel approach where photons are collected within a mirrored cylinder light collector in the forward (trans) direction after traversing the entire tissue absorptive path. This design minimizes light losses due to refractive index mismatch along the path to the wide-area detector by bathing the sample and detector interface with an index matching fluid (Crosignani et al., 2012, Crosignani et al., 2011). It is not yet clear how this approach will work in cases where the forward path to the detector is long and filled with absorptive biological elements such as the *in vivo* muscle and kidney studied in the current work.

In the almost uniquely transparent zebrafish sample, it was advantageous to place the sample on a mirror to optimize recovery of light that would have otherwise simply passed through (and away from) the animal. This type of sample might also be an ideal case for the arrangement proposed by Crosignani et al. 2011 and 2012, even without a mirror. A similar approach has been shown to be effective for other transparent samples (Rehberg *et al.*, 2010). We suggest, however, that small samples (few millimeters in size) that can fit on a 18 mm coverslip will best be imaged by the full total emission detection (full-TED) design which captures the *entire* solid angle of emission (Combs et al., 2007). The main limitation of either a flat or concave mirror beneath a translucent sample is that forward scattered light has to traverse the tissue a second time to get back to the detector. This incurs nearly twice the chance for absorption or uncollected scattering event. Clearly, if the sample and experimental design permits, the full-TED design, collecting most of the emitted light, is more desirable.

The previous epiTED (Combs et al., 2011), displayed a similar gain to c-TED. In most cases, both epiTED and c-TED collected slightly less light than was predicted by Monte Carlo simulations for the specialized case of an idealized highly scattering, relatively low light absorptive tissue (Combs et al., 2011). Part of this gain issue is explained by the wide aperture detector system we employed here. Even without the parabola, it is considerably more efficient than a normal objective based light collection system. Others have shown that significant gains in collection efficiency can be realized through efficient back aperture expansion systems that capture light originating from outside the point of geometric focus, thus increasing the effective N.A. of collection (Ducros *et al.*, 2011, Zinter & Levene, 2011). The large dichroic mirror in the nosepiece and light collection system of the c-TED arrangement has already realized gains akin to those revealed by Ducross et al. 2011 and Zinter and Levine et al. 2011 under our “control” conditions, without the parabola contribution (PMT aperture masking data not shown). Thus, our quoted gain factors for parabola addition are versus the ‘objective alone’ – but the latter includes the enhanced N.A. of collection realized within our wide aperture optical system. Even when ratioed against an enhanced version of ‘ objective alone’, gain values for the highly scattering fat tissue (with its low absorbance) was found to approach near-theoretical values of signal improvement (approaching 5 fold) at the surface (Figure 3C). Thus, the current design approaches the theoretical potential for total emission detection for some tissue types and geometries.

The main purpose of this study was to determine if the TED design could be miniaturized to the point where it would become a practical add-on to a conventional microscope and still provide gains comparable to the original bulky epiTED design. In addition, we wanted to minimize introduction of optical elements into the excitation path, to minimize aberrations that perturb the excitation point spread function. As the results demonstrate, we have achieved most of these goals, however our experience with this prototype of c-TED suggests further refinements could make this system more versatile and user-friendly. The size of the parabola opening would ideally be larger, to permit a wider range of applications and ease of positioning. For instance, doubling of the parabola aperture would be possible by increasing the optical power of the relay system -- reflecting the parabola-collected light by using matched toroidal rather than flat conical mirrors. Also, the conic telescope employed in this

first prototype was designed only to optimize a particular parabola-objective combination, where the universe of existing commercial water objectives was limiting. The best solution is to have an objective body and parabola designed together in a fixed unit (cf. Vucunic et al., 2006). Considerable advantage should accrue if one machines the objective body so that the region outside of the N.A. cone in the final lens is sloped and polished to direct all light to the parabola, obviating the need of the reflective collars used in this prototype. Pairings of parabolas with differing focal lengths (and hence openings) with appropriate conic telescopes is a straightforward process. Minor improvements in sample access (e.g. splitting the parabola into “petals” for opening and closing the structure) may also be helpful. The current prototype also did not have multi-channel capabilities, nor did it use the latest PMT technology for detection. Both of these modifications would be simple additions to this scheme and are not limited in any way by the c-TED geometry - outside of developing the appropriate optical guidepaths.

It is expected that the c-TED design could be useful for types of multi-photon excitation experiments other than the fluorescence and second harmonic generation imaging conducted here. The ability to exclusively recover photons that have diffused within the tissue before exiting is a prime advantage of TED. As pointed out by (Saar *et al.*, 2010), backscatter is the only practical route for forward CARS or SRS photons to exit tissue. Epi-CARS rapidly dephases in thick samples, so only forward CARS signals which subsequently backscatter are available to the microscope, and they dominantly exit at angles and positions unfavorable for conventional objectives to recover. TED will therefore likely become a useful accessory for CARS microscopes *in vivo*. Fluorescence Correlation spectroscopy (FCS) would also benefit from this design. To date, considerable expense and optical engineering has been devoted to the use of small-aperture APD (avalanche photodiode) detectors in the FCS method. While the timing/afterpulse characteristics of APDs are generally worse than PMTs, the undeniable doubling in QE (quantum efficiency) drives the choice. Both the full-TED approach (Combs et al., 2007) and epiTED devices (Combs et al., 2011) (more than) double the light available. Thus a PMT + TED system should provide detection efficiency equaling objective+APD. Fluorescence lifetime imaging (FLIM) may also benefit from this design, even though the longer paths from emitted spot to detector via parabola vs. objective might seem to confound FLIM. The central beam could, however, easily be delayed to compensate.

In summary, we have demonstrated a compact epiTED design (c-TED) compatible with a conventional turn-key upright MPEM. This design worked at least as well as previous, more complex and cumbersome designs. We confirmed earlier observations that a factor of two or better is realized in a variety of tissues using this approach with standard high N.A. water immersion lens. We also confirmed that the improvement in detection **decreased or remained the same** as a function of tissue depth in most samples, consistent with a dominant effect of scattering for longer light paths in most biological tissues. While the number of emitted photons that pass without deflection back through the objective to a *confocal* aperture will drop exponentially with depth, leading one to expect continuously rising gains with depth, real objectives with proximate, wide aperture detectors actually see a good portion of the diffuse light in the tissue. Thus gain (total with parabola/ wide aperture

objective) actually drops (or is nearly level) at greater depths. We confirmed this with Monte Carlo simulation (see supplemental information and accompanying figure S1). We also found that an earlier Monte Carlo simulation by Vucunic et al. (2006) for idealized hybrids predicted similar trends.

We intentionally chose our definition of gain to reflect only the improvement one could anticipate from c-TED over high aperture non-descanned detection.

From this experience, we suggest that optimally coupled parabolas (with appropriately modified objectives integrated within) will optimize the signal collecting characteristics of MPEM and make deep tissue imaging more robust.

## Supplementary Material

Refer to Web version on PubMed Central for supplementary material.

## Acknowledgments

This research was supported by the Intramural Research Program of the National Heart Lung and Blood Institute of the National Institutes of Health. We wish to thank Alan Hoofring and Ethan Tyler of the NIH Medical Illustration group for help preparing Figure 1 in this work. We also wish to thank Dr. Damian Dalle Nogare (NICHD, NIH) for donating Zebrafish embryos. We also wish to thank S. Gordon Aiken for in-house for help in testing and setting up the c-TED.

## References

Bakalar M, Schroeder JL, Pursley R, Pohida TJ, Glancy B, Taylor J, Chess D, Kellman P, Xue H, Balaban RS. Three-dimensional motion tracking for high-resolution optical microscopy, in vivo. J Microsc. 2012; 246:237–247. [PubMed: 22582797]

Centonze VE, White JG. Multiphoton excitation provides optical sections from deeper within scattering specimens than confocal imaging. Biophys J. 1998; 75:2015–2024. [PubMed: 9746543]

Combs CA, Smirnov A, Chess D, McGavern DB, Schroeder JL, Riley J, Kang SS, Lugar-Hammer M, Gandjbakhche A, Knutson JR, Balaban RS. Optimizing multiphoton fluorescence microscopy light collection from living tissue by noncontact total emission detection (epiTED). J Microsc. 2011; 241:153–161. [PubMed: 21118209]

Combs CA, Smirnov AV, Riley JD, Gandjbakhche AH, Knutson JR, Balaban RS. Optimization of multiphoton excitation microscopy by total emission detection using a parabolic light reflector. J Microsc. 2007; 228:330–337. [PubMed: 18045327]

Crosignani V, Dvornikov A, Aguilar JS, Stringari C, Edwards R, Mantulin WW, Gratton E. Deep tissue fluorescence imaging and in vivo biological applications. J Biomed Opt. 2012; 17:116023. [PubMed: 23214184]

Crosignani V, Dvornikov AS, Gratton E. Enhancement of imaging depth in turbid media using a wide area detector. J Biophotonics. 2011; 4:592–599. [PubMed: 21425242]

Denk W, Strickler JH, Webb WW. Two-photon laser scanning fluorescence microscopy. Science. 1990; 248:73–76. [PubMed: 2321027]

Ducros M, van 't Hoff M, Evrard A, Seebacher C, Schmidt EM, Charpak S, Oheim M. Efficient large core fiber-based detection for multi-channel two-photon fluorescence microscopy and spectral unmixing. J Neurosci Methods. 2011; 198:172–180. [PubMed: 21458489]

Engelbrecht CJ, Gobel W, Helmchen F. Enhanced fluorescence signal in nonlinear microscopy through supplementary fiber-optic light collection. Opt Express. 2009; 17:6421–6435. [PubMed: 19365467]

McMullen JD, Kwan AC, Williams RM, Zipfel WR. Enhancing collection efficiency in large field of view multiphoton microscopy. J Microsc. 2011; 241:119–124. [PubMed: 21118215]

McMullen JD, Zipfel WR. A multiphoton objective design with incorporated beam splitter for enhanced fluorescence collection. Opt Express. 2010; 18:5390–5398. [PubMed: 20389554]

Rehberg M, Krombach F, Pohl U, Dietzel S. Signal improvement in multiphoton microscopy by reflection with simple mirrors near the sample. J Biomed Opt. 2010; 15:026017. [PubMed: 20459262]

Rothstein EC, Carroll S, Combs CA, Jobsis PD, Balaban RS. Skeletal muscle NAD(P)H two-photon fluorescence microscopy in vivo: topology and optical inner filters. Biophys J. 2005; 88:2165–2176. [PubMed: 15596503]

Saar BG, Freudiger CW, Reichman J, Stanley CM, Holtom GR, Xie XS. Video-rate molecular imaging in vivo with stimulated Raman scattering. Science. 2010; 330:1368–1370. [PubMed: 21127249]

Schroeder JL, Luger-Hamer M, Pursley R, Pohida T, Chefd'hotel C, Kellman P, Balaban RS. Short communication: Subcellular motion compensation for minimally invasive microscopy, in vivo: evidence for oxygen gradients in resting muscle. Circ Res. 2010; 106:1129–1133. [PubMed: 20167928]

Vucinic D, Bartol TM Jr. Sejnowski TJ. Hybrid reflecting objectives for functional multiphoton microscopy in turbid media. Opt Lett. 2006; 31:2447–2449. [PubMed: 16880851]

Zinter JP, Levene MJ. Maximizing fluorescence collection efficiency in multiphoton microscopy. Opt Express. 2011; 19:15348–15362. [PubMed: 21934897]

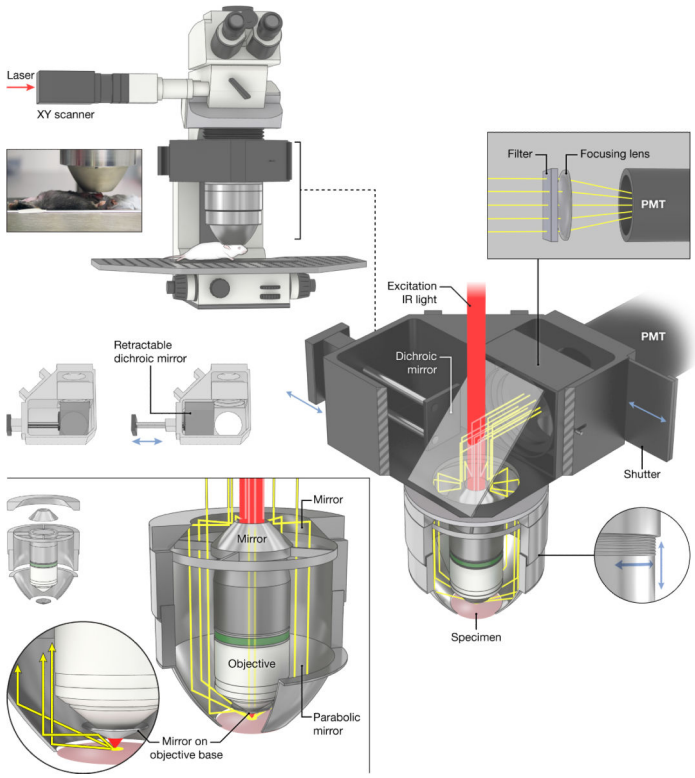


**Figure 1.**

The parabolic mirror assembly surrounds an objective on a regular commercially available upright two-photon microscope. Emission light collected by the parabola and the objective is reflected from a dichroic mirror in the turret and sent through an emission filter and focusing lens onto a wide-are PMT. The inset picture shows the relationship of the parabola to the sample for an experiment involving imaging of a leg muscle (Tibialis anterior). The dichroic mirror can be moved by a slider to enable standard wide-field imaging. Also shown is the thread system that allows focusing of the parabola.

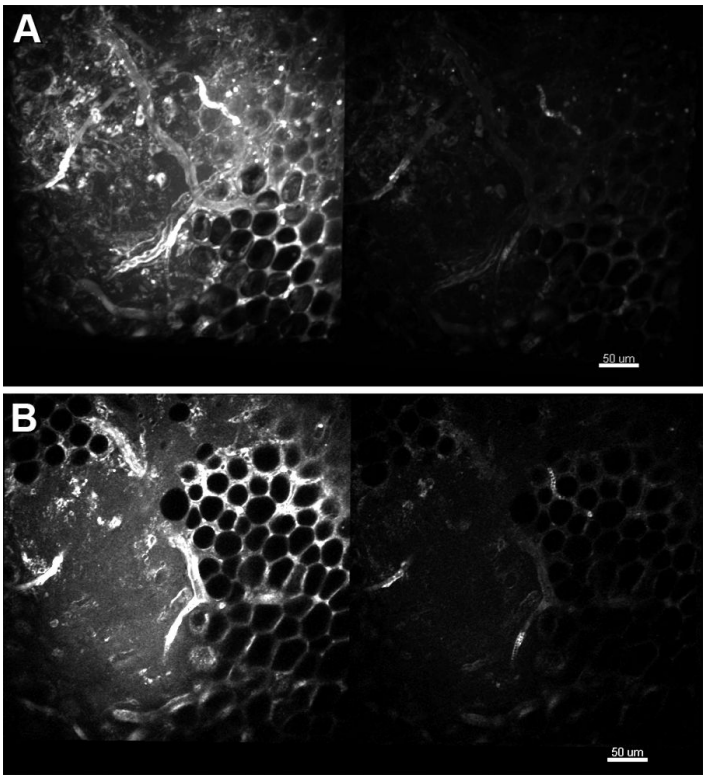


**Figure 2.**

Comparison of the compact TED collection efficiency and that of the objective alone for imaging fat and mixed tissue in murine skeletal muscle near the knee. **A**. Maximum intensity projection for the first 25 microns collected with the parabola and objective (left) and the objective alone (right). **B**. Single imaging plane from approximately 20 microns into the image stack depicted in A. Details of the imaging parameters can be found in “Materials and Methods”.

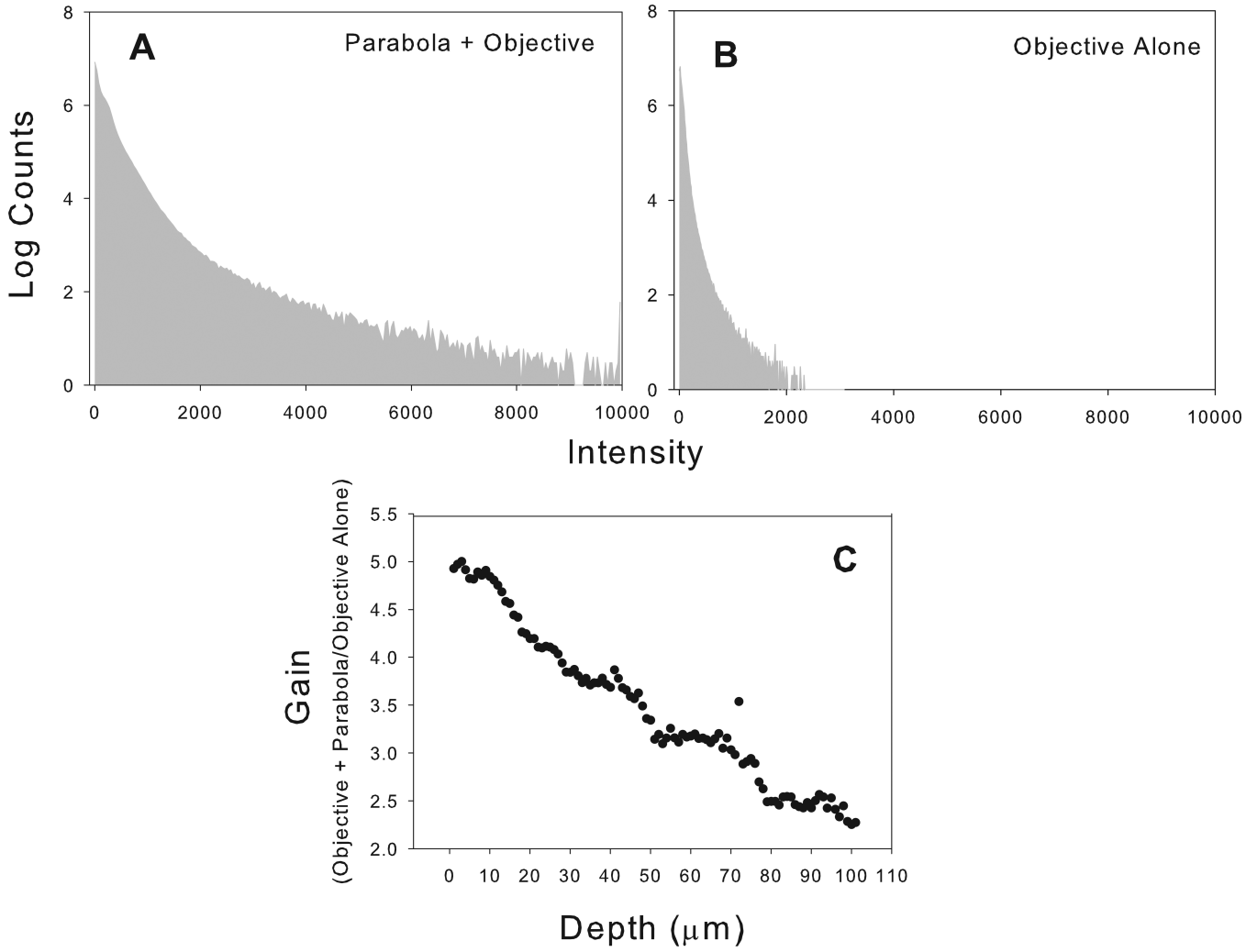


**Figure 3.**

Raw data of pixel intensities and gain by depth for the image stack depicted in figure 2A. **A** and **B** represent pixel histograms of intensities for the entire image stack depicted in 2A for c-TED and for the objective alone microscope configurations, respectively. **C**. Gain in collection efficiency as a function of imaging depth for the fat-dominated, mixed tissue depicted image shown in figure 2A.

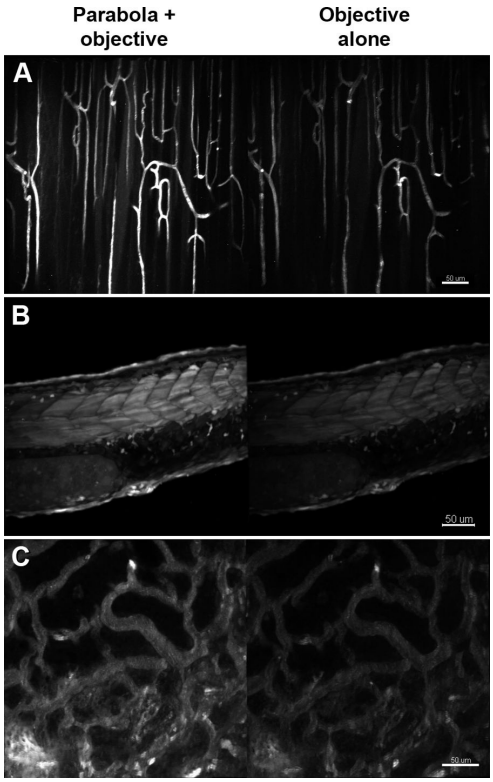


**Figure 4.**

Comparison of the c-TED collection efficiency (left) with that of the objective alone (right) for imaging three different types of tissues. **A**. Maximum intensity projections for a depth of 50 μm into skeletal for blood vessels labeled with di-8-ANNEPPS. **B**. Maximum intensity projections through the entire thickness (approximately 150 μm) of a zebrafish embryo expressing GFP. **C.** Maximum intensity projections for the first 25 μm through a live rat kidney labeled with di-8-ANNEPPS in the vasculature. Details of the imaging parameters can be found in “Materials and Methods”.

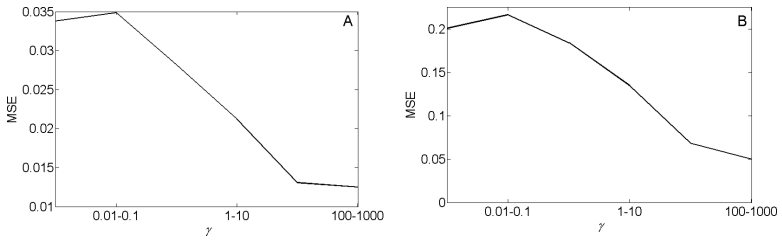


**Figure 5.**

The relationship between gain versus imaging depth. A. Gain versus depth for two mammalian tissues and a zebrafish embryo imaged *in vivo.* The zebrafish was imaged through its whole thickness (approximately 150 μm). The skeletal muscle was imaged to a depth of 300 μm whereas the kidney (a much more absorptive tissue) yielded useful images to a depth of approximately 200 μm. B. Linear false color montage images from various depths in a rat kidney for both the full c-TED and the objective alone configurations. The numbers in the top row of images correspond to the maximum intensity value in the cTED configuration and were used to byte-scale the images (to the false color inset on the right) for comparison between the two microscope configurations. Details of the analysis and the imaging parameters can be found in “Materials and Methods”.

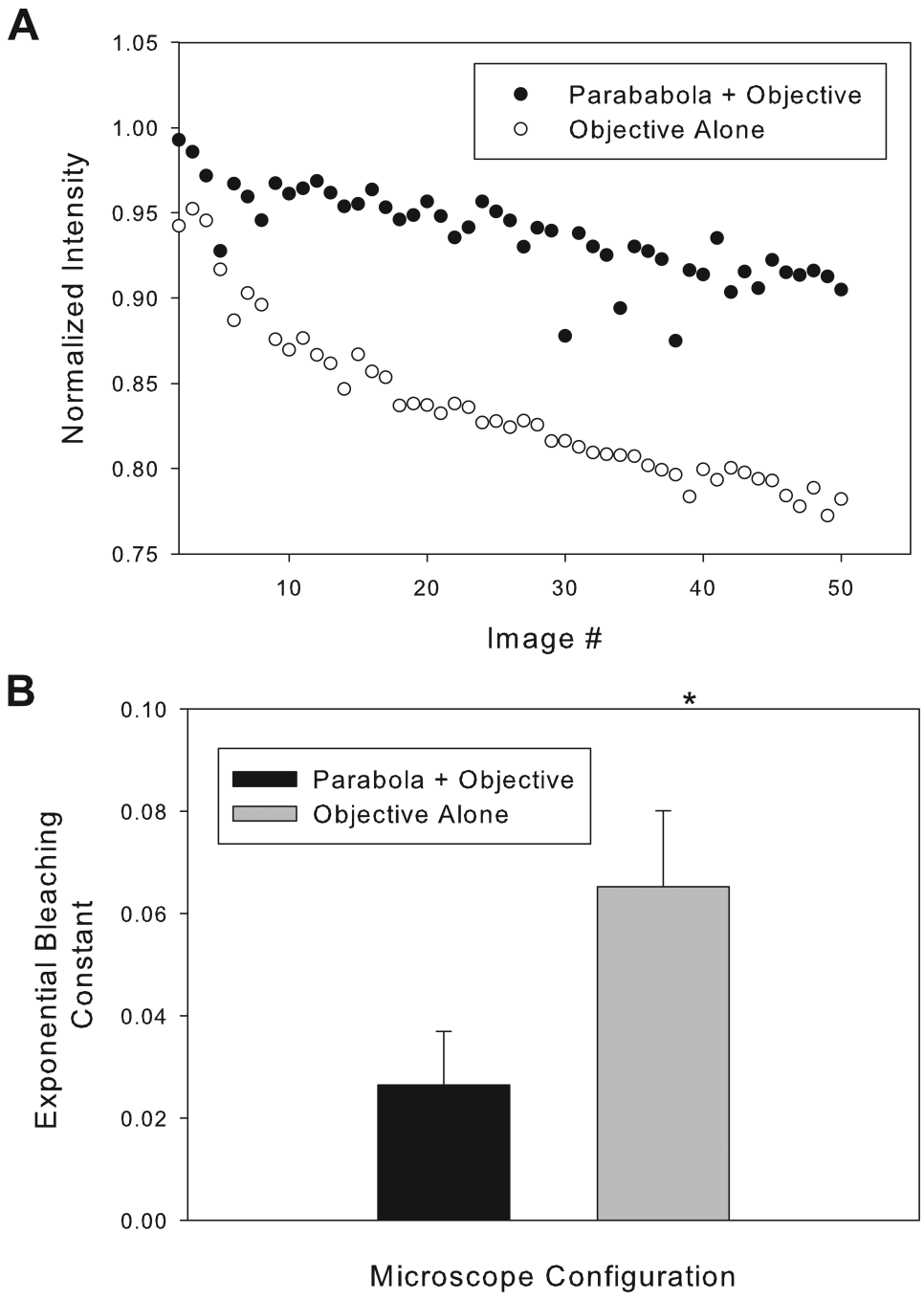


**Figure 6.**

Comparison of bleaching rates between the c-TED system and the objective alone for tetra methyl rhodamine (TMRM) labeled murine skeletal muscle imaged *in vivo*. Initial intensities were matched by changing excitation power. **A**. Raw intensity values over time for c-TED and the objective-alone microscope configurations from one representative experiment. **B.** Average calculated decay constants for repeated experiments (n=4). Details of the analysis and the imaging parameters can be found in “Materials and Methods”.